Chemical Geology 284 (2011) 262–269

Contents lists available at ScienceDirect

Chemical Geology

journal homepage: www.elsevier.com/locate/chemgeo

Experimental determination of solubility constant of hydromagnesite (5424) in NaCl solutions up to 4.4 m at room temperature ☆

Yongliang Xiong

Sandia National Laboratories (SNL), Carlsbad Programs Group, 4100 National Parks Highway, Carlsbad, NM 88220, USA

ARTICLE INFO

Article history:
Received 21 October 2010
Received in revised form 8 March 2011
Accepted 9 March 2011
Available online 14 March 2011

Editor: J. Fein

Keywords:
Hydromagnesite
Nuclear waste isolation
Geological repositories
CO_2 sequestration
Thermodynamics
Solubility study

ABSTRACT

This study reports the solubility constants of both synthetic and natural hydromagnesite (5424) determined in NaCl solutions with a wide range of ionic strength regarding the following reaction:

$$Mg_5(CO_3)_4(OH)_2 \cdot 4H_2O(cr) + 10H^+ \leftrightarrows 5Mg^{2+} + 4CO_2(g) + 10H_2O(l)$$

Solubility experiments were conducted from undersaturation in deionized water and 0.10–4.4 m NaCl solutions at P_{CO_2} of $10^{-3.4}$ atm and 22.5 °C, and lasting up to 1870 days. Based on the specific interaction theory, the weighted average solubility constant at infinite dilution calculated from the experimental results in 0.10–3.2 m NaCl solutions using the natural hydromagnesite (5424) from Staten Island, New York, is 58.39 ± 0.40 (2σ) in logarithmic units at 22.5 °C with a corresponding value of 57.93 ± 0.40 (2σ) at 25 °C. Similarly, the weighted average solubility constant using the natural hydromagnesite (5424) from Gabbs, Nevada, is 59.54 ± 0.72 (2σ) in logarithmic units at 22.5 °C with a corresponding value of 59.07 ± 0.72 (2σ) at 25 °C. The weighted average solubility constant of synthetic hydromagnesite (5424) determined from experiments in 0.10–4.4 m NaCl solutions is 61.53 ± 0.59 (2σ) in logarithmic units at 22.5 °C with a corresponding value of 61.04 ± 0.59 (2σ) at 25 °C. The natural hydromagnesite has lower solubilities because of its higher crystallinity related to their origins than synthetic hydromagnesite. The solubility constant of synthetic hydromagnesite is about one order of magnitude lower than the literature values. The Gibbs free energies of formation at the reference state (25 °C, 1 bar) are -5896 ± 2 kJ mol^{-1}, -5889 ± 4 kJ mol^{-1}, and $-5,878 \pm 3$ kJ mol^{-1} for the natural hydromagnesite from Staten Island, New York, from Gabbs, Nevada, and for the synthetic hydromagnesite, respectively.

1. Introduction

Industrial-grade MgO consisting mainly of the mineral periclase is the only engineered barrier certified by the Environmental Protection Agency (EPA) for emplacement in the Waste Isolation Pilot Plant (WIPP) in the U.S. (U.S. DOE, 1996, 2004), and an $Mg(OH)_2$-based engineered barrier consisting mainly of the mineral brucite is to be employed in the Asse repository in Germany (Schűessler et al., 2002). Therefore, the reaction path in the MgO-H_2O-CO_2 system (Xiong and Snider, 2003; Xiong and Lord, 2008) becomes important in nuclear waste management. The experimental studies in solutions up to ~7 M ionic strength at laboratory room temperature and atmospheric CO_2 have indicated that MgO is first hydrated as brucite, which in turn is carbonated as $Mg_5(CO_3)_4(OH)_2 \cdot 4H_2O$ (termed as hydromagnesite (5424) thereafter) (Xiong and Snider, 2003; Xiong and Lord, 2008). As MgO is in excess relative to CO_2 that may be produced, the brucite–hydromagnesite (5424) assemblage would buffer f_{CO_2} in the repository for considerable time before hydromagnesite (5424) converts to magnesite ($MgCO_3$). Consequently, the thermodynamic properties of this assemblage are of significance to the performance assessment (PA) as actinide solubility is strongly affected by f_{CO_2}. Therefore, accurate knowledge of thermodynamic properties of both brucite and hydromagnesite (5424) becomes important. Accordingly, the thermodynamic properties of brucite have recently been determined in a wide range of ionic strengths from both supersaturation and undersaturation (Xiong, 2003, 2008).

Geologically, sedimentary hydromagnesite has been observed in saline lakes in Australia, Canada, and Turkey (e.g., Last, 1992; Renaut, 1993; Braithwaite and Zedef, 1994; Camur and Mutlu, 1996; Zedef et al., 2000). The formation of hydromagnesite in karst caves has also been reported (Fischbeck and Müller, 1971). In addition, hydromagnesite is also observed as the very late stage constituents of the Mississippi Valley type (MVT) Pb–Zn deposit in the northern Pennine orefield, northern England (Green and Young, 2006). Therefore, the

☆ Sandia is a multiprogram laboratory operated by Sandia Corporation, a wholly owned subsidiary of Lockheed Martin Corporation, for the United States Department of Energy's National Nuclear Security Administration under contract DE-AC04-94AL85000.

E-mail address: yxiong@sandia.gov.

0009-2541/$ – see front matter © 2011 Elsevier B.V. All rights reserved.
doi:10.1016/j.chemgeo.2011.03.005

accurate knowledge of thermodynamic properties of hydromagnesite would also be useful in understanding the geochemical environments responsible for the formation of hydromagnesite under surface conditions as well as under hydrothermal conditions. In turn, such understanding would be highly relevant to sequestration of CO_2 in mafic and ultramafic rocks.

Previous studies on the thermodynamic properties of hydromagnesite were mainly conducted in the 1960's and 1970's (Table 1). Recently, hydromagnesite has attracted renewed interest from researchers in various fields because of its importance in nuclear waste isolation (e.g., Xiong and Snider, 2003; Xiong and Lord, 2008), its many industrial applications (e.g., Li et al., 2003), and its importance in CO_2 sequestration (e.g., Xiong and Lord, 2008). As mentioned in Xiong and Lord (2008), there are two stoichiometric formulas for hydromagnesite. One is hydromagnesite (5424) as mentioned above, and the other is $Mg_4(CO_3)_3(OH)_2 \cdot 3H_2O$, termed as hydromagnesite (4323) (Xiong and Lord, 2008). The natural occurrence of hydromagnesite (4323) is in Kozani, Greece (Stamatakis, 1995). It can be seen from Table 1 that there is a considerable discrepancy regarding the thermodynamic properties of hydromagnesite (5424) in the literature. For instance, the Gibbs free energy of formation varies from 5,859.8 to −5,896 kJ mol^{-1} with a difference of ~36 kJ mol^{-1} (Table 1). Similarly, the standard entropy in the literature ranges from 503.7 to 541.3 J mol^{-1} K^{-1} with a difference of ~38 J mol^{-1} K^{-1}. The thermodynamic properties given by Garrels et al. (1960), Langmuir (1965) and Wagman et al. (1982), refer to hydromagnesite (4323). There is also a considerable difference in terms of Gibbs free energy of formation for this phase. Therefore, it is desirable to redetermine the thermodynamic properties of hydromagnesite.

2. Methodology

Three starting materials were used in this study. The first starting material is the natural hydromagnesite from Basic Refractories Mine, near Gabbs, Nevada, purchased from Excalibur Mineral Company. The second starting material is the natural hydromagnesite from Staten Island, New York, purchased from Ward's Natural Science Company. The third starting material was synthesized from a solution started with deionized (DI) water and $Mg(OH)_2$ (brucite) at room temperature by sparging compressed atmospheric air into the solution. The synthetic and natural hydromagnesites have well defined XRD patterns (see Fig. 1). In comparison with the natural hydromagnesite, the synthetic hydromagnesite is not well crystalline as indicated by the relatively small peaks. The relatively low crystallinity is typical of the hydromagnesite synthesized at low temperatures including room temperature. For instance, the hydromagnesite synthesized at 30 °C has much less crystallinity than that heated at 55 °C (Fernández et al., 2000). It is also observed that the intensity for the peak of (011) (i.e., the peak at 2θ = ~15°) of the hydromagnesite synthesized at 50 °C is about two

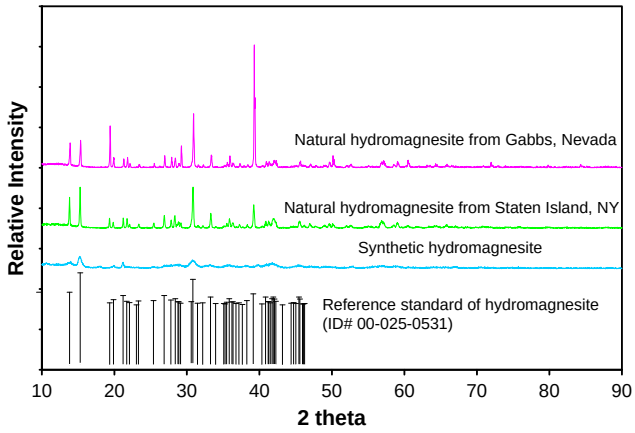

Fig. 1. XRD patterns of natural hydromagnesite from Staten Island, New York, and Gabbs, Nevada, and synthetic hydromagnesite, before experiments.

times less than that synthesized at 90 °C (Cheng and Li, 2010). The relatively high crystallinity of the natural hydromagnesite may be due to their origins. For instance, the hydromagnesite from Staten Island was formed during serpentinization by hydrothermal solutions (Julien, 1906, 1914). The hydromagnesite in association with huntite ($Mg_3Ca(CO_3)_4$) at Gabbs is suggested to have been formed by supergene alteration of brucite–magnesite ore bodies (Vitaliano and Beck, 1963; Schilling, 1967). The brucite–magnesite ore bodies occur in replacement bodies in the Triassic dolomite (Vitaliano and Callaghan, 1956). The formation of brucite–magnesite ore bodies is suggested to have been related the hydrothermal activity produced by the Mesozoic granitic intrusions (Schilling, 1968). Consequently, although the hydromagnesite from Gabbs was formed by the supergene processes, it would have been subject long formation time. Therefore, the synthetic hydromagnesite produced at room temperature in this study would be more relevant to the ambient conditions, especially on anthropogenic time scale. In this sense, it would be highly relevant to the time scale of the performance assessment of CO_2 sequestration.

There was no phase change during the experiments because XRD patterns at completion matched the initial XRD patterns (see Figs. 2–4). The XRD analyses were performed using a Bruker D8 Advance X-ray diffractometer with a Sol-X detector.

All reagents, including NaCl used for preparation of supporting solutions, and $Mg(OH)_2$ used for the synthesis of hydromagnesite, are reagent grade from Fisher Scientific. DI water at 18.3 MΩ was produced by a *NANOpure Infinity Ultra Pure Water System* from Barnstead. Stock solutions used for experiments from the direction of undersaturation with respect to hydromagnesite include DI water, 0.10 m, 1.0 m, 2.1 m, 3.2 m, and 4.4 m NaCl solutions. All experiments were conducted from undersaturation at the partial pressure of CO_2 of

Table 1
Literature values for thermodynamic properties of hydromagnesites at the reference state (25 °C and 1 bar).

Type of hydromagnesite	$\Delta_f G$ kJ mol^{-1}	$\Delta_f H$ kJ mol^{-1}	S^0 J mol^{-1} K^{-1}	Reference
Natural hydromagnesite(5424) from Hindubagh, Pakistan			503.67	Robie and Hemingway (1972)
Not specified	−5859.8			Robie and Hemingway (1973)
Not specified	−5864.6	−6514.9	541.3	Helgeson et al. (1978)
Not specified	−5864.2	−6514.9	503.7	Robie et al. (1978)
Synthetic hydromagnesite(5424)	−5871.5			Königsberger et al. (1992)
Synthetic hydromagnesite(5424)	−5870.5	−6516.0	520.0	Königsberger et al. (1999)
Natural hydromagnesite(5424) from Gabbs, NV	−5889 ± 4			This study
Natural hydromagnesite(5424) from Staten Island, NY	−5896 ± 2			This study
Synthetic hydromagnesite(5424)	−5878 ± 3			This study
Hydromagnesite(4323)	−4637.1			Garrels et al. (1960)
Hydromagnesite(4323)	−4602.8			Langmuir (1965)
Hydromagnesite(4323)	−4603.3			Wagman et al. (1982)

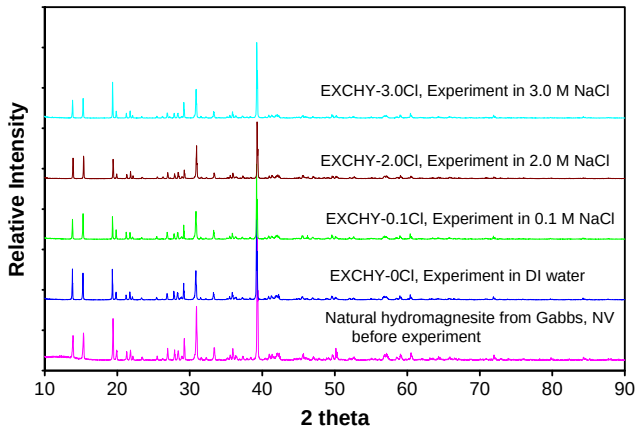

Fig. 2. XRD patterns of natural hydromagnesite from Gabbs, Nevada, before and after experiments.

$10^{-3.4}$ atm under a total pressure of one atmosphere. The mass of the natural hydromagnesite used in experiments ranges from 0.68 g to 1.3 g. The mass of the synthetic hydromagnesite employed in experiments ranges from 0.22 g to 0.49 g. The volume of solutions in experiments is about 200 mL.

All experiments were placed onto an INNOVA 2100 Platform Shaker (New Brunswick Scientific, Inc.) at a shaking speed of 140 RPM. All experiments were conducted at laboratory room temperature (22.5 ± 1.5 °C).

Before each sampling, the pH values of the experimental runs were measured. In each sampling, about 3 mL of solution was withdrawn from the experimental solutions, and was filtered with a 0.2 μm syringe filter. The filtered solution was then weighed, and acidified with 0.5 mL of concentrated TraceMetal® grade HNO_3 from Fisher Scientific, and diluted to a volume of 10 mL with DI water.

The pH was measured with an Orion-Ross combination pH glass electrode, using a pH meter that was calibrated with three pH buffers (pH 4, pH 7, and pH 10). In solutions with an ionic strength higher than 0.10 m, hydrogen-ion concentrations (pcH) instead of pH were determined from pH observed values from the pH glass electrode, as detailed in Xiong (2008) and Xiong and Lord (2008).

The chemical analyses of solutions were performed using a Perkin Elmer dual-view inductively coupled plasma-atomic emission spectrometer (ICP-AES) (Perkin Elmer DV 3300). The calibration blank and standards were precisely matched with experimental matrices. The correlation coefficients of calibration curves in all measurements were better than 0.9995. The analytical precision is better than 1.00% in terms of the relative standard deviation (RSD) based on replicate analyses.

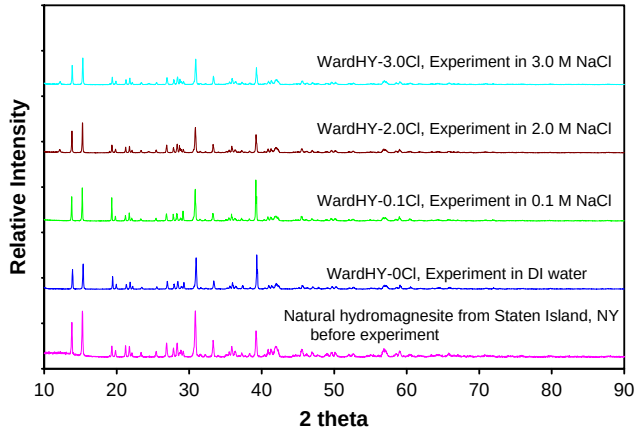

Fig. 3. XRD patterns of natural hydromagnesite from Staten Island, New York, before and after experiments.

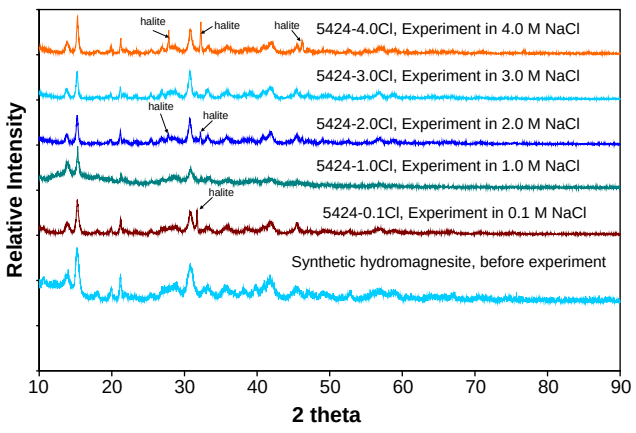

Fig. 4. XRD patterns of synthetic hydromagnesite produced in this study, before and after experiments. Notice that in some experimental products, when the synthetic hydromagnesite was dried at room temperature, residual NaCl solution, which was not completely removed, crystallized as halite (NaCl), as indicated by the peaks of halite.

3. Experimental results

Experimental results in DI water using natural hydromagnesite are listed in Table 2. All other experimental results in NaCl medium using natural and synthetic hydromagnesite are tabulated in Tables 3 and 4, respectively. In Fig. 5, concentrations of magnesium as a function of experimental time in experiments using the natural hydromagnesite are displayed. It seems that steady-state concentrations are reached in about 200 days in most experiments. Notice that the magnesium concentrations in the experiment of WardHY-2.0Cl are relative lower than those in the rest of experiments owing to the relatively lower hydrogen ion concentrations in that experiment (see Table 3). In Fig. 6, concentrations of magnesium as a function of time in experiments using the synthetic hydromagnesite as starting materials are shown. It also seems that steady-state concentrations are reached in about 200 days. It is assumed that steady-state concentrations reflect equilibrium state concentrations, as the duration of these experiments was significantly longer than was used in previous studies. In similar systems, for instance, equilibrium between brucite and solution was attained after about 83 days at room temperature (Xiong, 2008). In hydromagnesite (4323) solubility experiments from undersaturation at 25 °C conducted by Garrels et al. (1960), the authors mentioned that the equilibrium constants they obtained agree well with previous determinations for which reversals were attained. In the experiments of Garrels et al. (1960), the experimental duration was up to 4 days, and they extrapolated parameters such as pH to infinite time in the plot of concentrations versus the reciprocal of the square root of time ($\frac{1}{\sqrt{time}}$). In the eitelite ($NaMg_{0.5}CO_3$) solubility experiments from undersaturation at 25 °C conducted by Königsberger et al. (1992), the authors mentioned that constant e.m.f. readings in the cell system were obtained in 2 to 4 days, indicating that (metastable) equilibrium between eitelite and solution was attained. They refer to the dissolution of eitelite as a metastable equilibrium in their experiment. In pure water eitelite dissolves incongruently to form hydromagnesite. However, the incongruent dissolution was suppressed in their experiment in 3.0 m $NaClO_4$ because of the high concentration of Na^+. Therefore, because the experimental duration used in this study was much longer than that in the similar studies mentioned above, it is reasonable to assume that steady-state concentrations reported here are reflective of the equilibrium state.

In comparison with experiments using the natural hydromagnesite, concentrations of magnesium in experiments with the synthetic hydromagnesite are quite consistent over time. From Fig. 6, it also

Table 2
Experimental results in DI water using natural hydromagnesite at the partial pressure of CO_2 of $10^{-3.4}$ atm.

Experimental run number	Run time, day	pH	Ionic strength, m	$m_{Mg^{2+}}$	$\gamma_{Mg^{2+}}$	log K°[a]
ExcHy-0Cl[b]	31	8.83	4.60×10^{-3}	1.53×10^{-3}	0.739	59.97
	111	8.77	5.21×10^{-3}	1.74×10^{-3}	0.726	59.60
	120	8.79	5.74×10^{-3}	1.91×10^{-3}	0.715	59.98
	393	8.74	4.57×10^{-3}	1.52×10^{-3}	0.740	59.06
	412	8.79	5.34×10^{-3}	1.78×10^{-3}	0.723	59.85
	435	8.73	4.67×10^{-3}	1.56×10^{-3}	0.738	59.00
	486	8.74	7.26×10^{-3}	2.42×10^{-3}	0.687	59.90
	540	8.77	5.73×10^{-3}	1.91×10^{-3}	0.715	59.78
	615	8.76	5.08×10^{-3}	$1.69\pm0.00\times10^{-3}(2\sigma)$[c]	0.729	59.45
Average						$59.61\pm0.72(2\sigma)$
WardHy-0Cl[b]	111	8.78	5.47×10^{-3}	1.82×10^{-3}	0.720	59.79
	143	8.70	4.92×10^{-3}	1.64×10^{-3}	0.732	58.80
	150	8.77	5.41×10^{-3}	1.80×10^{-3}	0.722	59.67
	164	8.77	4.38×10^{-3}	1.46×10^{-3}	0.744	59.28
	181	8.74	6.36×10^{-3}	2.12×10^{-3}	0.703	59.67
	199	8.61	5.46×10^{-3}	1.82×10^{-3}	0.721	58.09
	247	8.62	6.90×10^{-3}	2.30×10^{-3}	0.693	58.61
	280	8.58	6.56×10^{-3}	2.19×10^{-3}	0.699	58.12
	304	8.62	6.73×10^{-3}	2.24×10^{-3}	0.696	58.57
	318	8.76	6.90×10^{-3}	$2.30\pm0.24\times10^{-3}(2\sigma)$[c]	0.700	60.01
	343	8.78	6.35×10^{-3}	$2.12\pm0.21\times10^{-3}(2\sigma)$[c]	0.700	60.06
	615	8.76	5.94×10^{-3}	$1.98\pm0.02\times10^{-3}(2\sigma)$[c]	0.710	59.74
Average						$59.2\pm1.4(2\sigma)$

[a] Equilibrium constants at infinite dilution (log K°) are computed by using measured pH and $m_{Mg^{2+}}$, and log $\gamma_{Mg^{2+}}$ calculated from the Davies equation.
[b] In the experimental run having "ExcHy-", the natural hydromagnesite from Gabbs, Nevada, purchased from Excalibur Mineral Company, was used as starting material. In the experimental run having "WardHy-", the natural hydromagnesite from Staten Island, New York, purchased from Ward's Natural Science Company, was used as starting material.
[c] Replicate analyses.

seems that there is a dependence of magnesium concentrations on ionic strength in experiments with the synthetic hydromagnesite. The magnesium concentrations in the experiment in 0.10 m NaCl (5424-0.1Cl) are lower than those in experiments with higher ionic strengths. However, this dependence is less obvious in the experiments with the natural hydromagnesites because the data are scattered to some degrees.

To obtain thermodynamic properties at infinite dilution from the above results, an extrapolation strategy was developed. The strategy of extrapolation to infinite dilution in this study is to use the Davies equation (Davies, 1938) to extrapolate experimentally determined equilibrium quotients at very low ionic strength (experiments starting with DI water) to infinite dilution, and to use the Specific Interaction Theory (SIT) model with interaction coefficients evaluated by Xiong (2006) to extrapolate the equilibrium quotients in NaCl solutions from 0.10 m to 4.4 m.

In this study, the standard state for a solid phase is defined as its pure end-member at 298.15 K and 1 bar. The standard state of an aqueous solute is defined as a hypothetical 1 molal solutions at 298.15 and 1 bar. The reference state of an aqueous solute is defined as "the limiting condition whereby the activity approaches the molal concentration as the concentration becomes infinitely dilute" (Nordstrom and Munoz, 1986).

The results obtained from the extrapolations by using the Davies equation and the SIT model are the dissolution constants for hydromagnesite as suggested below:

$$Mg_5(CO_3)_4(OH)_2\bullet 4H_2O(cr) + 10H^+ \rightleftharpoons 5Mg^{2+} + 4CO_2(g) + 10H_2O(l) \quad (1)$$

In the Davies equation, the activity coefficient is calculated from:

$$\log\gamma_i = -A_\gamma z_i^2\left(\frac{\sqrt{I_m}}{1+\sqrt{I_m}} + 0.3I_m\right) \quad (2)$$

where γ_i is the activity coefficient of *i* species; A_γ the Debye–Hückel slope for activity coefficient, and is from Helgeson and Kirkham (1974); z_i the charge of *i* species, and I_m ionic strength on molal scale.

The equilibrium constant for Reaction (1) is,

$$\begin{aligned} K &= \frac{\left(m_{Mg^{2+}}\right)^5\left(\gamma_{Mg^{2+}}\right)^5\left(P_{CO_2}\right)^4\left(\Gamma_{CO_2}\right)^4\left(a_{H_2O}\right)^{10}}{\left(m_{H^+}\right)^{10}\left(\gamma_{H^+}\right)^{10}} \\ &= \frac{\left(m_{Mg^{2+}}\right)^5\left(P_{CO_2}\right)^4}{\left(m_{H^+}\right)^{10}} \times \frac{\left(\gamma_{Mg^{2+}}\right)^5\left(\Gamma_{CO_2}\right)^4\left(a_{H_2O}\right)^{10}}{\left(\gamma_{H^+}\right)^{10}} \\ &= Q \times \frac{\left(\gamma_{Mg^{2+}}\right)^5\left(\Gamma_{CO_2}\right)^4\left(a_{H_2O}\right)^{10}}{\left(\gamma_{H^+}\right)^{10}} \end{aligned} \quad (3)$$

where $m_{Mg^{2+}}$ and m_{H^+} denote concentrations of Mg^{2+} and H^+ on molality scale, $\gamma_{Mg^{2+}}$ and γ_{H^+} activity coefficients of Mg^{2+} and H^+, respectively; P_{CO_2} and Γ_{CO_2} are partial pressure and fugacity coefficient of CO_2, respectively, and a_{H_2O} is the activity of water. The fugacity coefficient of CO_2 is taken as unity. In Eq. (3), the numerical combination of concentrations of Mg^{2+} and H^+ and partial pressure of CO_2 is equilibrium quotient (Q).

The extrapolation to infinite dilution regarding Reaction (1) using the SIT model is given by:

$$\log K_s^o = \log Q - 10D + \Delta\varepsilon\, I_m + 10\,\log a_{H_2O} \quad (4)$$

$$\Delta\varepsilon(\text{Eq.4}) = 5\varepsilon\left(Mg^{2+}, Cl^-\right) - 10\varepsilon\left(H^+, Cl^-\right) \quad (5)$$

where log Q is an equilibrium quotient regarding Reaction (1) at a certain ionic strength; $\varepsilon(Mg^{2+}, Cl^-)$ and $\varepsilon(H^+, Cl^-)$ are interaction coefficients of the BrØnsted–Guggenheim-Scatchard specific interaction theory estimated by Xiong (2006); a_{H_2O} is activity of water; and D is the Debye–Hückel term. The activities of water in NaCl solutions are from Robinson and Stokes (1959).

The Debye–Hückel term is given by:

$$D = \frac{A_\gamma\sqrt{I_m}}{1+\rho\sqrt{I_m}} \quad (6)$$

Table 3
Experimental results from the experimental runs in an NaCl medium using natural hydromagnesite as starting material at the partial pressure of CO_2 of $10^{-3.4}$ atm.

Experimental run number	Run time, day	pH_{ob}[a]	Ionic strength, m	m_{H^+}[b]	γ_{H^+}	$m_{Mg^{2+}}$	$\gamma_{Mg^{2+}}$	log Q	log K°[c]
ExcHy-0.1Cl	31	8.76	0.10	1.68×10^{-9}	0.801	2.00×10^{-3}	0.383	60.67	59.54
	66	8.67		2.06×10^{-9}		2.02×10^{-3}		59.78	58.65
	111	8.72		1.84×10^{-9}		1.96×10^{-3}		60.23	59.09
	120	8.70		1.92×10^{-9}		2.32×10^{-3}		60.39	59.26
	150	8.67		2.06×10^{-9}		2.05×10^{-3}		59.82	58.68
	164	8.65		2.16×10^{-9}		1.88×10^{-3}		59.43	58.29
	181	8.63		2.26×10^{-9}		2.27×10^{-3}		59.64	58.51
	615	8.68		2.01×10^{-9}		2.30×10^{-3}		60.17	59.03
Average								$60.02\pm0.83(2\sigma)$	$58.88\pm0.83(2\sigma)$
ExcHy-2.0Cl	88	8.56	2.1	1.33×10^{-9}	1.10	7.65×10^{-3}	0.323	64.57	61.38
	93	8.51		1.50×10^{-9}		5.17×10^{-3}		63.22	60.03
	126	8.53		1.43×10^{-9}		7.65×10^{-3}		64.27	61.08
	140	8.57		1.30×10^{-9}		4.67×10^{-3}		63.60	60.41
	165	8.50		1.53×10^{-9}		5.08×10^{-3}		63.08	59.89
	392	8.68		1.01×10^{-9}		4.86×10^{-3}		64.78	61.59
	462	8.66		1.06×10^{-9}		4.32×10^{-3}		64.33	61.14
	1871	8.68		1.01×10^{-9}		5.24×10^{-3}		64.95	61.76
								$64.1\pm1.4(2\sigma)$	$60.9\pm1.4(2\sigma)$
ExcHy-3.0Cl	11	8.58	3.2	8.64×10^{-10}	1.49	1.02×10^{-3}	0.482	62.07	58.23
	46	8.67		7.02×10^{-10}		2.07×10^{-3}		64.51	60.67
	126	8.49		1.06×10^{-9}		6.23×10^{-3}		65.11	61.27
	140	8.61		8.06×10^{-10}		3.80×10^{-3}		65.24	61.39
	151	8.58		8.64×10^{-10}		1.89×10^{-3}		63.42	59.57
	462	8.57		8.84×10^{-10}		4.27×10^{-3}		65.09	61.25
	970	8.60		8.25×10^{-10}		$5.14\pm0.00\times10^{-3}$		65.79	61.95
	1871	8.53		9.69×10^{-10}		9.69×10^{-3}		64.55	60.71
								$64.6\pm2.4(2\sigma)$	$60.8\pm2.4(2\sigma)$
WardHy-0.1Cl	31	8.83	0.10	1.43×10^{-9}	0.801	2.51×10^{-3}	0.383	61.86	60.72
	66	8.80		1.53×10^{-9}		2.73×10^{-3}		61.74	60.60
	111	8.78		1.60×10^{-9}		2.45×10^{-3}		61.31	60.17
	120	8.79		1.58×10^{-9}		2.93×10^{-3}		61.79	60.66
	129	8.80		1.53×10^{-9}		3.18×10^{-3}		62.07	60.94
	164	8.64		2.21×10^{-9}		1.82×10^{-3}		59.26	58.13
	181	8.72		1.84×10^{-9}		2.42×10^{-3}		60.68	59.54
	280	8.94		1.11×10^{-9}		1.53×10^{-3}		61.88	60.74
	615	8.80		1.53×10^{-9}		1.70×10^{-3}		60.71	59.57
Average								$61.3\pm1.8(2\sigma)$	$60.1\pm1.8(2\sigma)$
WardHy-2.0Cl	28	8.79	2.1	7.85×10^{-10}	1.10	6.57×10^{-4}	0.323	61.54	58.35
	93	8.79		7.85×10^{-10}		5.85×10^{-4}		61.29	58.09
	219	8.75		8.61×10^{-10}		7.05×10^{-4}		61.29	58.10
	322	8.79		7.85×10^{-10}		7.31×10^{-4}		61.77	58.58
	379	8.75		8.61×10^{-10}		7.28×10^{-4}		61.36	58.17
	499	8.78		8.03×10^{-10}		6.78×10^{-4}		61.51	58.31
	521	8.85		6.84×10^{-10}		4.34×10^{-4}		61.24	58.05
	567	8.83		7.16×10^{-10}		5.55×10^{-4}		61.57	58.38
	589	8.82		7.33×10^{-10}		7.10×10^{-4}		62.01	58.82
Average								$61.51\pm0.51(2\sigma)$	$58.32\pm0.51(2\sigma)$
WardHy-3.0Cl	28	8.43	3.2	1.22×10^{-9}	1.49	2.42×10^{-3}	0.482	62.46	58.62
	94	8.54		9.47×10^{-10}		4.19×10^{-3}		64.75	60.91
	127	8.44		1.19×10^{-9}		5.11×10^{-3}		64.18	60.33
	143	8.53		9.69×10^{-10}		3.39×10^{-3}		64.19	60.35
	392	8.55		9.26×10^{-10}		3.69×10^{-3}		64.57	60.73
	431	8.51		1.01×10^{-9}		3.77×10^{-3}		64.22	60.38
	462	8.41		1.28×10^{-9}		3.78×10^{-3}		63.22	59.38
	970	8.53		9.69×10^{-10}		$4.42\pm0.00\times10^{-3}$		64.76	60.92
Average								$64.1\pm1.6(2\sigma)$	$60.3\pm1.6(2\sigma)$

[a] pH observed values measured by using the pH glass electrode.
[b] Hydrogen ion concentration computed from the correction factors for corresponding pH observed values (see text for details).
[c] Equilibrium constants at infinite dilution (log K°) are computed from the SIT model.

where ρ is the minimum distance of approach between ions, which is taken as 1.5 (Ciavatta, 1980).

4. Calculation results and discussions

Based on the following equation for the calculation of weighted mean, the weighted average equilibrium constants at 22.5 °C are calculated (Table 5),

$$w_i = \frac{1}{\sigma_i^2} \tag{7}$$

$$\bar{X} = \frac{\sum_{i=1}^{n}\left(X_i/\sigma_i^2\right)}{\sum_{i=1}^{n} w_i} \tag{8}$$

where w_i is the weight of ith measurement, σ_i is the standard deviation of ith measurement. The variance of the weighted mean is computed from the following equation,

$$\sigma_{\bar{X}}^2 = \frac{1}{\sum_{i=1}^{n}\left(1/\sigma_i^2\right)}. \tag{9}$$

Table 4
Experimental results from the experimental runs in an NaCl medium using synthetic hydromagnesite as starting material at the partial pressure of CO_2 of $10^{-3.4}$ atm.

Experimental run number	Run time, day	pH_{ob}	Ionic strength, m	m_{H^+}	γ_{H^+}	$m_{Mg^{2+}}$	$\gamma_{Mg^{2+}}$	log Q	log K°[a]
5424-0.1Cl	111	8.88	0.1	1.27×10^{-9}	0.801	4.78×10^{-3}	0.383	63.75	62.62
	119	8.88		1.27×10^{-9}		2.81×10^{-3}		62.60	61.47
	161	8.89		1.24×10^{-9}		2.41×10^{-3}		62.37	61.23
	180	9.02		9.21×10^{-10}		1.77×10^{-3}		62.99	61.86
	231	8.76		1.68×10^{-9}		2.59×10^{-3}		61.23	60.09
	286	8.87		1.30×10^{-9}		1.83×10^{-3}		61.57	60.44
	432	8.97		1.03×10^{-9}		2.11×10^{-3}		62.88	61.75
	446	8.83		1.43×10^{-9}		2.54×10^{-3}		61.88	60.75
	474	8.83		1.43×10^{-9}		2.54×10^{-3}		61.88	60.75
	515	8.97		1.03×10^{-9}		3.35×10^{-3}		63.89	62.75
	526	8.93		1.13×10^{-9}		2.79×10^{-3}		63.09	61.96
	603	8.91		1.19×10^{-9}		3.41×10^{-3}		63.33	62.19
	624	8.92		1.16×10^{-9}		3.35×10^{-3}		63.39	62.25
	655	8.79		1.56×10^{-9}		3.05×10^{-3}		61.88	60.75
	670	8.93		1.13×10^{-9}		3.42×10^{-3}		63.53	62.39
	691	8.88		1.27×10^{-9}		2.63×10^{-3}		62.46	61.32
	714	8.83		1.43×10^{-9}		2.76×10^{-3}		62.06	60.93
	760	8.98		1.01×10^{-9}		3.33×10^{-3}		63.97	62.84
	770	8.98		1.01×10^{-9}		2.86×10^{-3}		63.64	62.51
Average								$62.8\pm1.7(2\sigma)$	$61.6\pm1.7(2\sigma)$
5424-1.0Cl	173	8.79	1.0	1.12×10^{-9}	0.849	4.05×10^{-3}	0.249	63.96	61.50
	203	8.69		1.40×10^{-9}		4.01×10^{-3}		62.94	60.48
	306	8.57		1.85×10^{-9}		4.90×10^{-3}		62.17	59.71
	315	8.69		1.40×10^{-9}		5.97×10^{-3}		63.80	61.34
	326	8.78		1.14×10^{-9}		4.03×10^{-3}		63.85	61.39
	343	9.01		6.72×10^{-10}		5.94×10^{-3}		61.99	59.53
	379	8.61		1.69×10^{-9}		4.46×10^{-3}		62.37	59.91
	714	8.84		9.94×10^{-10}		$5.88\pm0.21\times10^{-3}$		65.27 ± 0.08	62.81 ± 0.08
Average								$63.5\pm2.5(2\sigma)$	$61.1\pm2.5(2\sigma)$
5424-2.0Cl	10	8.92	2.1	1.20×10^{-9}	1.10	4.79×10^{-3}	0.323	64.00	60.81
	24	8.86		1.38×10^{-9}		4.58×10^{-3}		63.31	60.12
	93	8.83		1.48×10^{-9}		5.20×10^{-3}		63.28	60.09
	122	8.70		2.00×10^{-9}		9.05×10^{-3}		63.18	59.99
	133	8.77		1.70×10^{-9}		5.89×10^{-3}		62.95	59.76
	186	8.72		1.91×10^{-9}		6.75×10^{-3}		62.75	59.56
	218	8.73		1.86×10^{-9}		8.76×10^{-3}		63.41	60.22
	410	8.88		1.32×10^{-9}		6.46×10^{-3}		64.25	61.06
	431	8.92		1.20×10^{-9}		6.12×10^{-3}		64.53	61.34
	498	8.88		1.32×10^{-9}		7.24×10^{-3}		64.50	61.31
	521	8.77		1.70×10^{-9}		5.34×10^{-3}		62.74	59.55
	528	8.90		1.26×10^{-9}		6.51×10^{-3}		64.47	61.28
	1871	8.95		1.12×10^{-9}		4.73×10^{-3}		63.88	60.69
Average								$63.6\pm1.3(2\sigma)$	$60.4\pm1.3(2\sigma)$
5424-3.0Cl	10	8.92	3.2	1.20×10^{-9}	1.49	5.80×10^{-3}	0.482	64.42	60.58
	24	8.90		1.26×10^{-9}		5.05×10^{-3}		63.92	60.08
	38	9.07		8.51×10^{-10}		6.16×10^{-3}		66.05	62.21
	322	8.76		1.74×10^{-9}		9.03×10^{-3}		63.78	59.94
	333	8.75		1.78×10^{-9}		7.95×10^{-3}		63.40	59.56
	448	8.75		1.78×10^{-9}		6.98×10^{-3}		63.12	59.28
	498	8.73		1.86×10^{-9}		8.27×10^{-3}		63.29	59.45
	567	8.81		1.55×10^{-9}		6.00×10^{-3}		63.39	59.55
	577	8.78		1.66×10^{-9}		7.92×10^{-3}		63.69	59.86
	588	8.81		1.55×10^{-9}		8.40×10^{-3}		64.12	60.28
	647	8.80		1.58×10^{-9}		8.76×10^{-3}		64.11	60.27
	969	8.73		1.86×10^{-9}		$8.19\pm0.00\times10^{-3}$		63.27	59.43
Average								$63.6\pm1.6(2\sigma)$	$60.4\pm1.6(2\sigma)$
5424-4.0Cl	144	8.54	4.4	6.29×10^{-9}	2.07	$4.21\pm0.24\times10^{-3}$	0.774	66.54 ± 0.13	62.04 ± 0.13
	151	8.54		6.29×10^{-9}		$4.70\pm0.51\times10^{-3}$		66.77 ± 0.24	62.27 ± 0.24
	180	8.60		5.48×10^{-9}		$5.07\pm0.29\times10^{-3}$		67.54 ± 0.12	63.04 ± 0.12
	217	8.54		6.29×10^{-9}		4.98×10^{-3}		66.90	62.41
	231	8.56		6.01×10^{-9}		6.51×10^{-3}		67.68	63.19
	260	8.47		7.39×10^{-9}		5.90×10^{-3}		66.57	62.07
	271	8.44		7.92×10^{-9}		6.69×10^{-3}		66.54	62.04
	358	8.45		7.74×10^{-9}		6.61×10^{-3}		66.62	62.12
	379	8.49		7.06×10^{-9}		5.31×10^{-3}		66.54	62.04
	411	8.53		6.44×10^{-9}		7.35×10^{-3}		67.65	63.15
	580	8.52		6.59×10^{-9}		5.68×10^{-3}		66.99	62.49
	624	8.53		6.44×10^{-9}		4.77×10^{-3}		66.71	62.21
	655	8.46		7.56×10^{-9}		5.59×10^{-3}		66.35	61.86
	714	8.55		6.15×10^{-9}		4.97×10^{-3}		67.00	62.50
	810	8.55		6.15×10^{-9}		4.29×10^{-3}		66.68	62.18
Average								$66.88\pm0.86(2\sigma)$	$62.39\pm0.86(2\sigma)$

[a] Equilibrium constants at infinite dilution (log K°) are computed from the SIT model.

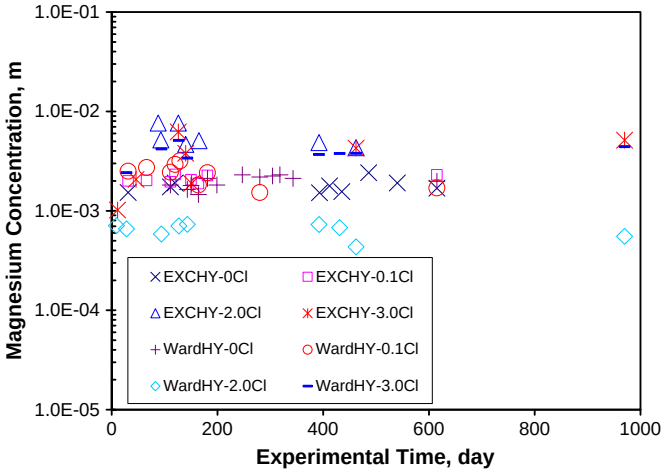

Fig. 5. A plot showing magnesium concentrations as a function of experimental time in experiments using the natural hydromagnesite as a starting material.

According to the above equations, the weighted average solubility constants determined in NaCl medium at 22.5 °C for the natural hydromagnesite from Staten Island, New York, and from Gabbs, Nevada, are 58.39 ± 0.40 (2σ) and 59.54 ± 0.72 (2σ) in logarithmic unit, respectively (Table 5). These values are in excellent agreement with those determined in experiments started with DI water (Table 2). For the synthetic hydromagnesite, its weighted solubility constant determined in NaCl medium is 61.53 ± 0.59 (2σ) (Table 5). From Table 5, it is obvious that natural hydromagnesites from both Gabbs, Nevada, and Staten Island, New York, have lower solubility than the synthetic hydromagnesite. In the study of Königsberger et al. (1999), they also indicated that the natural magnesite ($MgCO_3$) has lower solubility than the synthetic magnesite.

Based on equilibrium constants at 22.5 °C, the equilibrium constants at 25 °C are calculated from the following equation for temperature variations of Gibbs free energy, assuming constant heat capacity over this temperature range,

$$\Delta G^o_T = \Delta G^o_{298.15} - (T-298.15)\Delta S^o_{298.15} + \int_{298.15}^{T} \Delta C^o_p dT - T\int_{298.15}^{T} \Delta C^o_p d\ln T \quad (10)$$

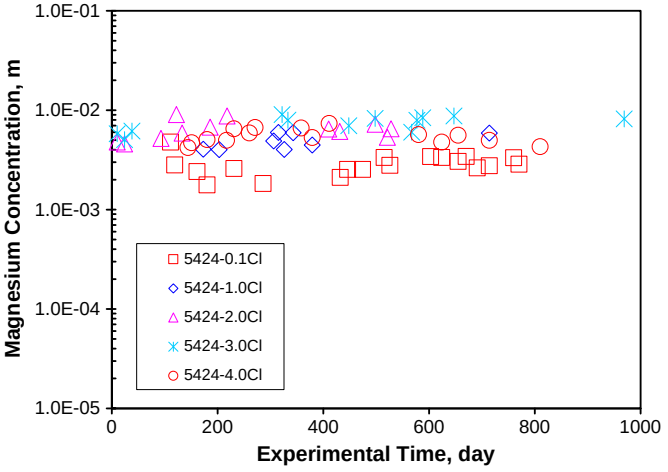

Fig. 6. A plot showing magnesium concentrations as a function of experimental time in experiments using the synthetic hydromagnesite as a starting material.

Table 5
Average solubility constants of hydromagnesite (5424) at infinite dilution at 22.5 °C based on results determined in NaCl medium from 0.1 m to 4.4 m, and corresponding values extrapolated to 25 °C.

Solid phase	log K ± 2σ at 22.5 °C[a]	log K ± 2σ at 25 °C
Gabbs (NV) hydromagnesite	59.54 ± 0.72	59.07 ± 0.72
Staten Island (NY) hydromagnesite	58.39 ± 0.40	57.93 ± 0.40
Synthetic hydromagnesite	61.53 ± 0.59	61.04 ± 0.59

[a] The average equilibrium constants and associated uncertainties are calculated based on the equations for weighted mean and its variance in which weights are computed from experimental uncertainties listed in Tables 3–4. The equations are listed in the text.

where Gibbs free energy can be calculated from a equilibrium constant by using the following expression,

$$\log K_T = -\frac{\Delta G^0_T}{\ln 10 \times RT}. \quad (11)$$

In the calculation, entropies of H_2O (l), CO_2 (g) and Mg^{2+} are from Königsberger et al. (1999), and of hydromagnesite is from Robie and Hemingway (1972). Heat capacities of H_2O (l) and CO_2 (g) are from Königsberger et al. (1999), and those of Mg^{2+} and hydromagnesite are from Desnoyers et al. (1976) and from Robie and Hemingway (1972), respectively. The equilibrium constants in logarithmic units at 25 °C are also listed in Table 5.

Based on the equilibrium constants at 25 °C, the Gibbs free energies of formation of hydromagnesite are derived (Table 1). In comparison with the literature values, the Gibbs free energy of the synthetic hydromagnesite is similar to, but still slightly more negative than, that provided by Königsberger et al. (1992, 1999). However, the Gibbs free energies of the natural hydromagnesite are considerably more negative than the literature values.

As mentioned in Xiong (2008) and Xiong and Lord (2008), magnesite is the thermodynamically stable phase, metastable hydromagnesite (5424) is the most likely phase to be formed in the repositories in which MgO or $Mg(OH)_2$ are employed as an engineered barrier to sequestrate CO_2. Therefore, the f_{CO_2} will be buffered by the assemblage brucite–hydromagnesite (5424) in the early history of the WIPP. However, hydromagnesite (5424) is expected to be converted to magnesite ($MgCO_3$) in the 10,000-year period, which is the performance period for the repository set by the EPA.

Based on the solubility constants of hydromagnesite determined in this study, in combination with the solubility constant of brucite determined in Xiong (2008), the evolution of f_{CO_2} buffered by the assemblage of brucite–hydromagnesite with the increasing crystallinity of hydromagnesite can be assessed. The solubility constant of brucite at 25 °C for the following reaction,

$$Mg(OH)_2(cr) + 2H^+ = Mg^{2+} + 2H_2O(l) \quad (12)$$

is determined as 17.05 ± 0.20 (2σ) (Xiong, 2008). Combination of Reaction (12) with Reaction (1) yields,

$$5Mg(OH)_2(cr) + 4CO_2(g) = Mg_5(CO_3)_4(OH)_2\cdot 4H_2O(cr) \quad (13)$$

According to the solubility constants of hydromagnesite determined in this study, the log f_{CO_2} buffered by Reaction (13) can be

Table 6
Comparison of log f_{CO_2} buffered by the assemblage of brucite–hydromagnesite for the natural and synthetic hydromagnesite at 25 °C.

Hydromagnesite	log f_{CO_2}, bars
Natural hydromagnesite, Staten Island, NY	−6.83 ± 0.11
Natural hydromagnesite, Gabbs, NV	−6.55 ± 0.19
Synthetic hydromagnesite	−6.05 ± 0.16

calculated. In Table 6, log f_{CO_2} buffered by brucite with hydromagnesite with various crystallinity is listed. The log f_{CO_2} buffered by brucite-synthetic hydromagnesite is -6.05 ± 0.16 (2σ) bars. When crystallinity increases, the log f_{CO_2} would decrease to -6.83 ± 0.11 (2σ) bars. Therefore, if the thermodynamic properties of synthetic hydromagnesite are used for calculations, the results would be conservative.

5. Summary

In this study, the solubility constants of the natural and synthetic hydromagnesite have been determined in a wide range of ionic strengths in an NaCl medium. The solubility constant of the natural hydromagnesite from Staten Island, New York, which was formed by the hydrothermal processes, is 57.93 ± 0.40 (2σ) at 25 °C, close to the value of 59.07 ± 0.72 (2σ) at 25 °C for the hydromagnesite from Gabbs, Nevada, which was formed by the supergene alteration of brucite–magnesite ore bodies, taking the quoted uncertainties into consideration. The solubility constant of the synthetic hydromagnesite is 61.04 ± 0.59 (2σ) at 25 °C, which is slightly higher than that for the natural hydromagnesite. The lower solubility of the natural hydromagnesites is attributed to their higher crystallinity, which is related to their origins. The f_{CO_2} buffered by the assemblage of brucite–hydromagnesite would be expected to decrease when the crystallinity of hydromagnesite increases with time, which would be favorable to the performance of geological repositories.

Acknowledgments

Sandia National Laboratories is a multiprogram laboratory operated by Sandia Corporation, a wholly owned subsidiary of Lockheed Martin Corporation, for the United States Department of Energy's National Nuclear Security Administration under Contract DE-AC04-94AL85000. This research is funded by WIPP programs administered by the Office of Environmental Management (EM) of the U.S Department of Energy. My thanks are due to Nathalia Chadwick, Kelsey Mae Davis, and Veronica Gonzales, for their laboratory assistance. The author wishes to dedicate this work to Kelsey Mae Davis, who passed away on June 12, 2006, in appreciation of her assistance. The author is grateful to Dr. I-Ming Chou and another journal reviewer for their detailed and thoughtful reviews, and to Dr. Jeremy Fein for his editorial efforts and comments. Their efforts significantly improved the presentation of the manuscript.

References

Braithwaite, C.J.R., Zedef, V., 1994. Living hydromagnesite stromatolites from Turkey. Sedimentary Geology 92, 1–5.
Camur, M.Z., Mutlu, H., 1996. Major-ion geochemistry and mineralogy of the Salt Lake (Tuz Gölü) basin, Turkey. Chemical Geology 127, 313–329.
Cheng, W.-T., Li, Z.-B., 2010. Controlled supersaturation precipitation of hydromagnesite for the $MgCl_2$-Na_2CO_3 system at elevated temperatures: chemical modeling and experiment. Industrial and Engineering Chemistry Research 49, 1964–1974.
Ciavatta, L., 1980. The specific interaction theory in evaluating ionic equilibria. Annali di Chimica 70, 551–567.
Davies, C.W., 1938. The extent of dissociation of salts in water. VIII. An equation for the ionic activity coefficients of an electrolyte in water, and a revision of the dissociation constant of some sulfates. Journal of Chemical Society 2093–2098.
Desnoyers, J.E., de Visser, C., Perron, G., Picker, P., 1976. Reexamination of the heat capacities obtained by flow microcalorimetry: recommendation for the use of a chemical standard. Journal of Solution Chemistry 5, 605–616.
Fernández, A.I., Chimenos, J.M., Segarra, M., Fernández, M.A., Espiell, F., 2000. Procedure to obtain hydromagnesite from a MgO-containing residue, kinetic study. Industrial and Engineering Chemistry Research 49, 1964–1974.
Fischbeck, R., Müller, G., 1971. Monohydrocalcite, hydromagnesite, nesquehonite, dolomite, aragonite, and calcite in speleothems of the Fräinkische Schweiz, Western Germany. Contributions to Mineralogy and Petrology 33, 87–92.
Garrels, R.M., Thompson, M.E., Siever, R., 1960. Stability of some carbonates at 25 °C and one atmosphere total pressure. American Journal of Science 258, 402–418.
Green, D.I., Young, B., 2006. Hydromagnesite and dypingite from the Northern Pennine Orefield, northern England. Proceedings of the Yorkshire Geological Society 56, 151–154.
Helgeson, H.C., Kirkham, D.H., 1974. Theoretical prediction of the thermodynamic behavior of aqueous electrolytes at high pressures and temperatures. II. Debye–Hückel parameters for activity coefficients and relative partial molal properties. American Journal of Sciences 274, 1199–1261.
Helgeson, H.C., Delany, J.M., Nesbitt, W.H., Bird, D.K., 1978. Summary and critique of the thermodynamic properties of rock-forming minerals. American Journal of Science 278-A 229 pp.
Julien, A.A., 1906. The occlusion of igneous rock within metamorphic schists, as illustrated on and near Manhattan Island, New York. Annals of the New York Academy of Sciences 16, 387–446.
Julien, A.A., 1914. The genesis of antigorite and talc. Annals of the New York Academy of Sciences 24, 23–38.
Königsberger, E., Schmidt, P., Gamsjäger, H., 1992. Solid-solute phase equilibria in aqueous solution. VI. Solubilities, complex formation, and ion-interaction parameters for the system Na^+–Mg^{2+}–ClO_4–CO_2–H_2O at 25 °C. Journal of Solution Chemistry 21, 1195–1216.
Königsberger, E., Königsberger, L.C., Gamsjäger, H., 1999. Low-temperature thermodynamic model for the system Na_2CO_3–$MgCO_3$–$CaCO_3$–H_2O. Geochimica et Cosmochimica Acta 63, 3105–3119.
Langmuir, D., 1965. Stability of carbonates in the system MgO–CO_2–H_2O. Journal of Geology 73, 730–754.
Last, W.M., 1992. Petrology of modern carbonate hardgrounds from East Basin Lake, a saline maar lake, southern Australia. Sedimentary Geology 81, 215–229.
Li, Q., Ding, Y., Yu, G.-H., Li, C., Li, F.-Q., Qian, Y.-T., 2003. Fabrication of light-emitting porous hydromagnesite with rosette-like architecture. Solid State Communication 125, 117–120.
Nordstrom, D.K., Munoz, J.L., 1986. Geochemical Thermodynamics. Blackwell Scientific Publications, Boston, MA. 477 pp.
Renaut, R.W., 1993. Morphology, distribution, and preservation potential of microbial mats in the hydromagnesite-magnesite playas of the Cariboo Plateau, British Columbia, Canada. Hydrobiologia 267, 75–98.
Robie, R.A., Hemingway, B.S., 1972. The heat capacities at low-temperatures and entropies at 298.15 K of nesquehonite, $MgCO_3 \cdot 3H_2O$, and hydromagnesite. American Mineralogist 57, 1768–1781.
Robie, R.A., Hemingway, B.S., 1973. The enthalpies of nesquehonite, $MgCO_3 \cdot 3H_2O$, and hydromagnesite, $5MgO \cdot 4CO_2 \cdot 5H_2O$. US Geological Survey Journal of Research 1 (5), 543–547.
Robie, R.A., Hemingway, B.S., Fisher, J.R., 1978. Thermodynamic properties of minerals and related substances at 298.15 K and 1 bar (105 Pascals) pressure and at higher temperatures. U.S. Geological Survey Bulletin, 1452. 456 pp.
Robinson, R.A., Stokes, R.H., 1959. Electrolyte Solutions. Butterworths Scientific Publications, London.
Schilling, J.H., 1967. Artinite from Gabbs, Nevada: a correction for location. American Mineralogist 52, 889.
Schilling, J.H., 1968. The Gabbs magnesite–brucite deposit, Nye County, Nevada. In: Ridge, J.D. (Ed.), Ore Deposits of the United States, 1933–1967: Graton-Sales, 2. American Institute of Mining, Metallalurgical and Petroleum Engineers, New York, pp. 1608–1621.
Schűessler, W., Metz, V., Kienzler, B., Vejmelka, P., 2002. Geochemically based source term assessment for the Asse salt mine: comparison of modeling and experimental results (abstract). Programs and Abstracts of Materials Research Society Annual Meeting at Boston, MA, p. 713.
Stamatakis, M.G., 1995. Occurrence and genesis of huntite–hydromagnesite assemblages, Kozani, Greece—important new white fillers and extenders. Transaction of the Institution of Mining and Metallurgy, Section B: Applied Earth Science 104, B179–B186.
U.S. DOE, 1996. . DOE/CAO 1996–2184 Title 40 CFR Part 191 Compliance Certification Application. Appendix SOTERM. U.S. DOE Carlsbad Area Office, Carlsbad, NM.
U.S. DOE, 2004. Title 40 CFR Part 191 Compliance Recertification Application for the Waste Isolation Pilot Plant, Vol. 1–8. U.S. DOE Carlsbad Field Office, Carlsbad, NM. DOE/WIPP 2004–3231.
Vitaliano, C.J., Beck, C., 1963. Artinite, Gabbs, Nevada. American Mineralogist 48, 1158–1163.
Vitaliano, C.J. and Callaghan, E., 1956, *Geologic map of the Gabbs magnesite and brucite deposits, Nye County, Nevada*: U.S. Geological Survey Mineral Investigations Field Studies Map, MF-35.
Wagman, D.D., Evans, W.H., Parker, V.B., Schumm, R.H., Halow, I., Bailey, S.M., Churney, K.L., Buttall, R.L., 1982. The NBS tables of chemical thermodynamic properties. Selected values for inorganic and C1 and C2 organic substances in SI units. Journal of Physical Chemistry Reference Data 11 (Suppl. 2), 392.
Xiong, Y.-L., 2003. Revised thermodynamic properties of brucite determined by solubility studies and its significance to nuclear waste isolation. Abstracts with Programs, Geological Society of America Annual Meeting (Seattle, Washington, November 2–5, 2003), 35(6), pp. 102–103.
Xiong, Y.-L., 2006. Estimation of medium effects on equilibrium constants in moderate and high ionic strength solutions at elevated temperatures by using specific interaction theory (SIT): interaction coefficients involving Cl^-, OH^- and Ac^- up to 200 degrees C and 400 bars. Geochemical Transactions 7, 4. doi:10.1186/1467-4866-7-4.
Xiong, Y.-L., 2008. Thermodynamic properties of brucite determined by solubility studies and their significance to nuclear waste isolation. Aquatic Geochemistry 14, 223–238.
Xiong, Y.-L., Lord, A.S., 2008. Experimental investigations of the reaction path in the MgO–H_2O–CO_2 system in solutions with various ionic strengths, and their applications to nuclear waste isolation. Applied Geochemistry 23, 1634–1659. doi:10.1016/j.apgeochem.2007.12.035.
Xiong, Y.-L., Snider, A.C., 2003. Experimental investigations of the reaction path in the system MgO–H_2O–CO_2 in concentrated brines at ambient temperature and ambient laboratory atmospheric CO_2: applications to the Waste Isolation Pilot Plant. 2003 Radiochemistry Conference, July 13–16, 2003, Carlsbad, New Mexico, USA.
Zedef, V., Russell, M.J., Fallick, A.E., Hall, A.J., 2000. Genesis of vein stockwork and sedimentary magnesite and hydromagnesite deposits in the ultramafic terranes of southwestern Turkey: a stable isotope study. Economic Geology 95, 429–445.